Imaging the uptake of gold nanoshells in live cells using plasmon resonance enhanced four wave mixing microscopy

Natalie Garrett,[1,*] Matt Whiteman,[2] and Julian Moger[1]

[1]*School of Physics, University of Exeter, Exeter, Devon, EX4 4QL, UK*
[2]*Peninsula Medical School, University of Exeter, St. Luke's Campus, Exeter, Devon, UK*
**n.l.garrett@exeter.ac.uk*

Abstract: Gold nanoshells (GNS) are novel metal nanoparticles exhibiting attractive optical properties which make them highly suitable for biophotonics applications. We present a novel investigation using plasmon-enhanced four wave mixing microscopy combined with coherent anti-Stokes Raman scattering (CARS) microscopy to visualize the distribution of 75 nm radius GNS within live cells. During a laser tolerance study we found that cells containing nanoshells could be exposed to < 2.5 mJ each with no photo-thermally induced necrosis detected, while cell death was linearly proportional to the power over this threshold. The majority of the GNS signal detected was from plasmon-enhanced four wave mixing (FWM) that we detected in the epi-direction with the incident lasers tuned to the silent region of the Raman spectrum. The cellular GNS distribution was visualized by combining the epi-detected signal with forwards-detected CARS at the CH_2 resonance. The applicability of this technique to real-world nanoparticle dosing problems was demonstrated in a study of the effect of H_2S on nanoshell uptake using two donor molecules, NaHS and GYY4137. As GYY4137 concentration was increased from 10 μM to 1 mM, the nanoshell pixel percentage as a function of cell volume (PPCV) increased from 2.15% to 3.77%. As NaHS concentration was increased over the same range, the nanoshell PPCV decreased from 12.67% to 11.47%. The most important factor affecting uptake in this study was found to be the rate of H_2S release, with rapid-release from NaHS resulting in significantly greater uptake.

OCIS codes: (180.4315) Nonlinear microscopy; (170.1530) Cell analysis; (300.6230) Spectroscopy, coherent anti-Stokes Raman scattering; (160.4236) Nanomaterials.

References and links

1. C. L. Nehl, H. Liao, and J. H. Hafner, "Optical properties of star-shaped gold nanoparticles," Nano Lett. **6**(4), 683–688 (2006).
2. S. J. Oldenburg, J. B. Jackson, S. L. Westcott, and N. J. Halas, "Infrared extinction properties of gold nanoshells," Appl. Phys. Lett. **75**(19), 2897–2899 (1999).
3. J. Yang, J. Lee, J. Kang, S. J. Oh, H.-J. Ko, J.-H. Son, K. Lee, J.-S. Suh, Y.-M. Huh, and S. Haam, "Smart drug-loaded polymer gold nanoshells for systemic and localized therapy of human epithelial cancer," Adv. Mater. (Deerfield Beach Fla.) **21**(43), 4339–4342 (2009).
4. N. J. Durr, T. Larson, D. K. Smith, B. A. Korgel, K. Sokolov, and A. Ben-Yakar, "Two-photon luminescence imaging of cancer cells using molecularly targeted gold nanorods," Nano Lett. **7**(4), 941–945 (2007).
5. L. Tong, Q. Wei, A. Wei, and J.-X. Cheng, "Gold nanorods as contrast agents for biological imaging: optical properties, surface conjugation and photothermal effects," Photochem. Photobiol. **85**(1), 21–32 (2009).
6. S. E. McNeil, "Nanotechnology for the biologist," J. Leukoc. Biol. **78**(3), 585–594 (2005).
7. K. Bogunia-Kubik and M. Sugisaka, "From molecular biology to nanotechnology and nanomedicine," Biosystems **65**(2-3), 123–138 (2002).
8. S. W. Bishnoi, C. J. Rozell, C. S. Levin, M. K. Gheith, B. R. Johnson, D. H. Johnson, and N. J. Halas, "All-optical nanoscale pH meter," Nano Lett. **6**(8), 1687–1692 (2006).

#150556 - $15.00 USD Received 5 Jul 2011; revised 18 Aug 2011; accepted 19 Aug 2011; published 22 Aug 2011

9. J. C. Y. Kah, R. C. Y. Wan, K. Y. Wong, S. Mhaisalkar, C. J. R. Sheppard, and M. Olivo, "Combinatorial treatment of photothermal therapy using gold nanoshells with conventional photodynamic therapy to improve treatment efficacy: an in vitro study," Lasers Surg. Med. **40**(8), 584–589 (2008).
10. X. Huang, W. Qian, I. H. El-Sayed, and M. A. El-Sayed, "The potential use of the enhanced nonlinear properties of gold nanospheres in photothermal cancer therapy," Lasers Surg. Med. **39**(9), 747–753 (2007).
11. C. Leatherdale, W.-K. Woo, F. V. Mikulec, and M. G. Bawendi, "On the absorption cross section of CdSe nanocrystal quantum dots," J. Phys. Chem. B **106**, 7619–7622 (2002).
12. J. Park, A. Estrada, K. Sharp, K. Sang, J. A. Schwartz, D. K. Smith, C. Coleman, J. D. Payne, B. A. Korgel, A. K. Dunn, and J. W. Tunnell, "Two-photon-induced photoluminescence imaging of tumors using near-infrared excited gold nanoshells," Opt. Express **16**(3), 1590–1599 (2008).
13. J. Park, A. Estrada, J. A. Schwartz, J. D. Payne, A. K. Dunn, and J. W. Tunnell, "3D Microscopy of gold nanoshells in tumors using two-photon-induced photoluminescence," in *Plasmonics in Biology and Medicine V* (2008), Vol. 6869, p. L8690.
14. L. Tong and J.-X. Cheng, "Label-free imaging through nonlinear optical signals," Mater. Today **14**(6), 264–273 (2011).
15. C. L. Evans and X. S. Xie, "Coherent anti-stokes Raman scattering microscopy: chemical imaging for biology and medicine," Annu Rev Anal Chem (Palo Alto Calif) **1**(1), 883–909 (2008).
16. L. G. Rodriguez, S. J. Lockett, and G. R. Holtom, "Coherent anti-stokes Raman scattering microscopy: a biological review," Cytometry A **69**(8), 779–791 (2006).
17. A. Volkmer, J. X. Cheng, and X. S. Xie, "Vibrational imaging with high sensitivity via epidetected coherent anti-Stokes Raman scattering microscopy," Phys. Rev. Lett. **87**(2), 023901 (2001).
18. J. Moger, B. D. Johnston, and C. R. Tyler, "Imaging metal oxide nanoparticles in biological structures with CARS microscopy," Opt. Express **16**(5), 3408–3419 (2008).
19. M. Whiteman, L. Li, P. Rose, C.-H. Tan, D. B. Parkinson, and P. K. Moore, "The effect of hydrogen sulfide donors on lipopolysaccharide-induced formation of inflammatory mediators in macrophages," Antioxid. Redox Signal. **12**(10), 1147–1154 (2010).
20. L. Li, M. Whiteman, Y. Y. Guan, K. L. Neo, Y. Cheng, S. W. Lee, Y. Zhao, R. Baskar, C.-H. Tan, and P. K. Moore, "Characterization of a novel, water-soluble hydrogen sulfide-releasing molecule (GYY4137): new insights into the biology of hydrogen sulfide," Circulation **117**(18), 2351–2360 (2008).
21. G. J. Thomas, Jr., "Raman spectroscopy of protein and nucleic acid assemblies," Annu. Rev. Biophys. Biomol. Struct. **28**(1), 1–27 (1999).
22. Y. Jung, H. Chen, L. Tong, and J. X. Cheng, "imaging gold nanorods by plasmon-resonance-enhanced four wave mixing," J. Phys. Chem. C **113**(7), 2657–2663 (2009).
23. H. Kim, D. K. Taggart, C. Xiang, R. M. Penner, and E. O. Potma, "Spatial control of coherent anti-stokes emission with height-modulated gold zig-zag nanowires," Nano Lett. **8**(8), 2373–2377 (2008).
24. C. Liu and B. Q. Li, "Computational multiscattering of spherical multilayered gold nanoshells," J. Phys. Chem. C **115**(13), 5323–5333 (2011).

1. Introduction

Our understanding of the sub-cellular biological processes is largely founded upon microscopy-based investigations that require stains and tags such as fluorescent labels for contrast. Few traditional contrast agents provide the required resolution, specificity or sensitivity over sub-cellular length scales without adversely perturbing the chemical environment of the sample. Additional problems such as photobleaching and phototoxicity also hamper such experiments. Recent developments in nanotechnology have produced specialized gold nanoparticles (GNPs) that provide contrast at intensities equaling or in some cases surpassing that of fluorescent labels, without the associated drawbacks.

GNPs are well suited to biological applications as they are non-toxic and their chemically unreactive properties make them highly stable in biological environments. There are numerous approaches to engineering GNPs of different morphologies such as nanostars [1], nanorods and nanoshells [2] with diverse potential biomedical applications including: drug-delivery platforms [3], enhanced image contrast agents [4] and nanoscale probes that track the motion of cells and individual molecules [5]. Of these GNPs, it is perhaps gold nanoshells (GNS) that have attracted the most interest for use in biophotonics since they are highly reproducible and have appealing optical properties for biological applications. GNS are spherical nanoparticles that consist of a dielectric core surrounded with a continuous layer of gold that have nano-scale diameters. Their nanoscale size enables them to readily interact with cells, often in ways which do not alter the intrinsic biochemical processes [6,7], but perhaps even more interesting is their behavior under exposure to light.

#150556 - $15.00 USD Received 5 Jul 2011; revised 18 Aug 2011; accepted 19 Aug 2011; published 22 Aug 2011

Gold nanoshells can be tailored to efficiently absorb light under illumination wavelengths at or near to their plasmon resonance, a property exploited in a range of applications including photothermal treatment of cancer and subcellular pH sensing [8–10]. Because they may be engineered to preferentially absorb or scatter light in the near infrared, GNS can exploit the NIR "window" of optimal light penetration into tissue. Additionally, GNS have optical cross sections that may be up to 140 times greater than fluorescent beads, while emitting light at the same order of magnitude of brightness as nano-rods and up to twice that of CdSe QDs [11], with the added advantage that they do not experience photo-bleaching or "blinking". The intense photoluminescence of GNS has been exploited in experiments using them as contrast agents both under linear excitation and non-linear regimes using Multiphoton Induced Luminescence (MIL) [12,13]. Non-linear excitation schemes offer many advantages for bio-imaging as they typically employ near infrared wavelengths, they reduce photodamage and phototoxicity whilst allowing increased depth penetration into scattering media. Moreover, the nonlinear signal dependence provides intrinsic "confocal-like" spatial resolution.

When investigating the cellular uptake of GNPs it is important to co-localize particle location with the cellular structure. Therefore, a single imaging modality for identifying and spatially localizing GNPs within live cells is desirable. However, signals from these nanoparticles have been estimated as being approximately three orders of magnitude brighter than intrinsic autoflourescence for cellular structures [4]. Relying on auto-fluorescence in such detection schemes therefore allows visualization of nanoparticles with only limited information regarding biological morphology. We demonstrate that with four wave mixing (FWM) microscopy it is possible to visualize the distribution of GNS whilst simultaneously generating label-free contrast of surrounding cellular structures. FWM is a third-order non-linear optical process and is sensitive to $\chi^{(3)}$. In FWM microscopy, three incident fields with frequencies of ω_1, ω_2, ω_3 interact with the material to generate a signal field at a frequency of ω_4. FWM is sensitive to both the vibrational and electronic properties of the material. Vibrationally enhanced FWM is achieved when the wavenumber difference between the excitation fields matches a molecular vibration; this is used in coherent anti-Stokes Raman scattering (CARS). Electronically enhanced FWM occurs when one (or more) of the four fields is resonant with an electronic transition within the material. This effect is particularly significant in nanomaterials [14]. For experimental simplicity degenerate FWM is commonly employed in which $\omega_2 = \omega_3$ and the FWM signal, $\omega_{FWM} = 2\omega_1 - \omega_2$. In the case of degenerate CARS the vibrationally resonant signal, ω_{CARS}, occurs when $\omega_1 - \omega_2$ matches a vibrational resonance. In this case ω_1 and ω_2 are referred to as the pump (ω_p) and Stokes (ω_S) frequencies respectively.

Both CARS and FWM microscopy have been proved to be powerful tools for providing images of biological samples [15–17]. The information obtained in FWM images is dependent on the detection geometry. Phase matching criteria dictate that scatterers within the sample that are smaller than the incident wavelength may produce stronger FWM signals than bulk scatterers in the back-detected (epi) direction, whereas larger structures provide better contrast in forwards-detected FWM [17]. The suitability of epi-detected FWM for investigating nanoparticles within biological structures has already been demonstrated by Moger *et al* when imaging ZnO particles in fish gills using electronically resonant FWM [18]. Although chemically specific, the CARS signal exhibits a non-resonant component that is present both on and off the Raman-active resonance. This non-resonant background is significantly diminished in epi-detected CARS for aqueous samples since signal from the bulk water is effectively cancelled out by destructive interference [19]. We show that we can detect forwards-CARS contrast from live cells simultaneously with plasmon-enhanced epi-detected FWM signal from GNS, allowing the 3D distribution of GNS to be correlated with the cellular sub-structures. We investigate the dependence of nanoshell mediated photo-thermal induced cell damage on incident laser power and demonstrate that there exists a threshold incident power within which it is possible to image GNS inside cells without inducing damaging

#150556 - $15.00 USD Received 5 Jul 2011; revised 18 Aug 2011; accepted 19 Aug 2011; published 22 Aug 2011

photo-thermal effects. By imaging below the threshold, we were able to map the 3D spatial distribution of GNS within live cancer and macrophage cell cultures.

In order to demonstrate the ability of FWM imaging to study factors affecting cellular uptake of nanoparticles, we determined the phagocytosis of GNS in macrophages under exposure to two chemicals that release hydrogen sulfide at different rates. Just as nitric oxide and carbon monoxide were once thought of merely as metabolic poisons but are now recognized as having important biological mediating properties, hydrogen sulfide (H_2S) is now being regarded in the same light. Although H_2S is known to be an important endogenous gas with cardiovascular signaling properties, there is much conflicting data on its exact role in inflammation. Experiments investigating the effects of H_2S on inflammation, phagocytosis and other cellular processes have largely relied upon rapid-release donor molecules such as NaHS, which releases H_2S immediately in aqueous solutions. This rapid release of H_2S induces effects in cells that are not found *in vivo*, where the gas is typically released at much slower rates and at lower concentrations [20,21]. Recent investigations of an alternative water-soluble H_2S-releasing compound [morpholin-4-ium 4 methoxyphenyl(morpholino) phosphinodithioate (GYY4137)] have found that it releases H_2S at rates comparable to those *in vivo* and that both the concentration and rate of release of H_2S elicit different responses in inflammatory processes [20,21].

As yet there are no published studies on the effect of GYY4137 on particle uptake in cell cultures. We exposed macrophage cells to a range of concentrations of GYY4137 and NaHS before incubating with GNS and used FWM imaging to compare the relative volumes of cell cytoplasm containing GNS. We found that when exposed to the rapid-donor NaHS, the volume of cell cytoplasm containing FWM signal from GNS was between 3 and 5 times greater than when exposed to the slow-donor GYY4137. This study indicates that the rate of H_2S release has an important role in phagocytosis and demonstrates the suitability of GNS for use as cellular contrast agents in FWM imaging.

2. Materials and methods

2.1 FWM microscopy

The FWM optical setup is illustrated schematically in Fig. 1. For the pulsed laser source, a Levante OPO (Levante Emerald, APE, Berlin) pumped with a neodymium vanadate source. The Nd:Vanadate source (High-Q Picotrain, Hohenems, Austria) provides a 6 ps pulse width laser beam with a wavelength of 1064 nm which is frequency doubled to 532 nm. The power from this source is up to 10 W with a repetition rate of 76 MHz. The OPO converts the incoming 532 nm pump beam into two outputs (the signal and idler beams) which are required for CARS generation. These pump (signal) and Stokes (idler) beams are tunable from 690 to 990 nm and 1150 to 2300 nm respectively.

Imaging was achieved using modified commercial inverted microscope (IX71, Olympus UK) and confocal scan unit (FV300, Olympus UK). The pump and Stokes beams were focused on the sample using a water immersion objective lens (UPLSAPO 60 x 1.2 NA, Olympus, UK). The forward-propagating FWM signal was collected by an air condenser (NA = 0.55), band-pass filtered (HQ750/210, Chroma Technologies) to isolate the FWM signal and detected by a photomultiplier tube (R3896, Hamamatsu). The epi-FWM signal was collected using the objective lens, separated from the excitation beams by a long-wave pass dichroic mirror (z850rdc-xr, Chroma Technologies) and detected at the rear microscope port by a second PMT to perform imaging, or a spectrometer (Andor, Shamrock sr-303 and iDus CCD) to study the FWM emission spectra.

#150556 - $15.00 USD Received 5 Jul 2011; revised 18 Aug 2011; accepted 19 Aug 2011; published 22 Aug 2011

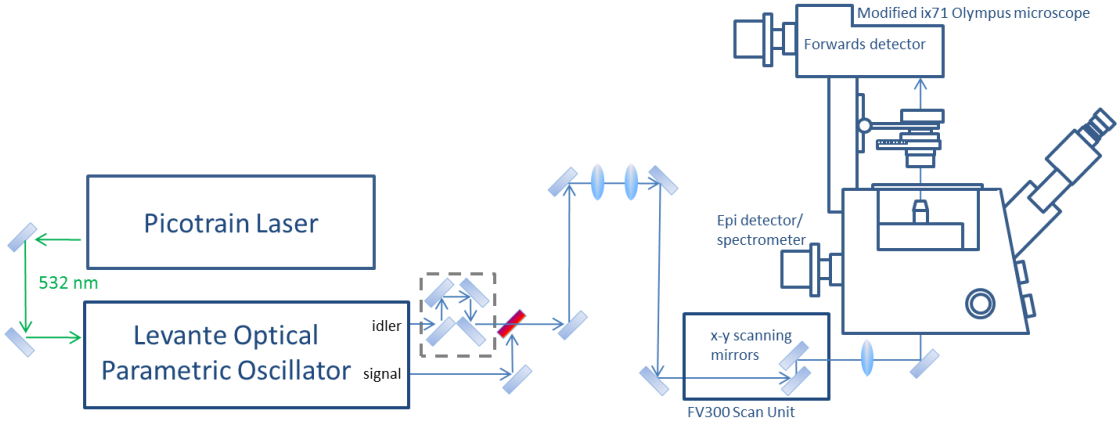

Fig. 1. Schematic diagram of the FWM microscopy optical layout.

Since GNS could be found throughout the cell cytoplasm, it was necessary to image entire cell volumes in 3D. Three-dimensional data were acquired by taking stacks of 2D images in the x-y plane each separated by an increment in the z-direction, which was achieved by altering the height of the objective relative to the sample. The microscope stage was enclosed in a temperature-controlled environmental chamber (Life Imaging Services, Switzerland), maintained at a constant temperature of 37 °C in order to maintain cell viability during image acquisition.

2.2. Gold nanoshells

GNS (nanoComposix, San Diego) were supplied with an optical resonance at 785 nm (core diameter 120 nm, gold shell thickness 15 nm +/– 0.4 nm). Diameter and shell integrity were verified by Scanning Electron Microscopy (Hitachi, S-3200N). Absorption spectra of GNS suspended in cell culture medium were obtained on a UV/visible light spectrophotometer (Biochrom Ultrospec 4300 pro, Cambridge, England) with quartz cuvettes of 2 mm path length, using an identical cuvette containing culture medium alone as a control.

2.3 Cell culture and nanoparticle exposure

Mouse monocyte macrophage cells (RAW264.7, European Collection of Cell Cultures) were cultured in Dulbecco's modified Eagle's medium (DMEM, Lonza) supplemented with 10% Fetal Bovine Serum (FBS) (S1900/500, Biosera, UK) and 0.2% Gentamicin (G1397, Sigma Aldrich) by volume. RAW264.7 cells were cultured until 80% confluent, passaged and then split 1:4. After splitting and plating up onto Fluorodish cell culture dishes (World Precision Instruments, UK), cells were maintained at 37 °C and 5% CO_2 for 24 hours prior to imaging. Human epidermoid carcinoma cells (A431, London School of Pharmacy, UK) were grown in DMEM supplemented with 10% FBS, 1% L-glutamine (Lonza), 1% minimal essential medium non-essential amino acids (MEMaa, Lonza) by volume at 37°C and 5% CO_2 and were cultured on Fluorodishes using the same procedure as the macrophage cells.

The GNS were supplied in an aqueous solution, aliquots of which were taken prior to experimentation and sonicated in a bath sonicator (Ultrawave, UK) for 20 minutes before being centrifuged at 4000 rpm for 5 minutes. GNS were then re-suspended in DMEM and sonicated again. Cell cultures were seeded overnight onto Fluorodishes containing 2 mL macrophage growth medium with 0.2 x 10^6 cells per dish before exposure to GNS in DMEM. The medium was gently aspirated to facilitate even distribution of GNS throughout the culture dishes. Mouse macrophages were also exposed to 8μL lipopolysaccharide (LPS) (K-235, Sigma Aldrich) immediately after addition of GNS in order to activate phagocytic response.

#150556 - $15.00 USD Received 5 Jul 2011; revised 18 Aug 2011; accepted 19 Aug 2011; published 22 Aug 2011

Once the required inoculation time had lapsed, the cells were subsequently rinsed 5 times in fresh DMEM to remove excess GNS.

Cultures exposed to GNS were examined under white light microscopy (Leica DMLFS upright microscope) for morphological changes, e.g. changes in cell division rates or membrane morphology, and were tested using Trypan blue stain (0.4%, Lonza) to determine any variation in the cell mortality rates. No significant changes were observed over a period of 24 hours with GNS doses of up to 1 x 10^8 GNS/mL, which corresponds to approximately 300 GNS per cell.

To investigate potential effects of excitation powers on cell viability, 2 mL of Trypan blue was added to the cell culture medium for 10 minutes after FWM imaging. The medium was then gently aspirated and replaced with fresh PBS. Further images were taken of the regions scanned under FWM using white light microscopy, in order to identify the cells that had taken up the Trypan blue. The percentage of cells containing the blue dye was determined by comparison of "before", "during" and "after" images.

Two H_2S donors were used to investigate the effect of the rate of hydrogen disulfide release on particle phagocytosis. The first, a rapid-release donor, NaHS (Sigma Aldrich). The second, a slow-release donor, GYY4137, of molecular weight 367.5 was manufactured as described previously [20]. Briefly, morpholine (20 mMol) in methyl chloride (CH2Cl2, 6 mL) was added drop wise at room temperature to a CH_2Cl_2 solution (6 mL) of 2,4-bis(4-methoxyphenyl)-2,4-dithioxo-1,3,2,4-dithiadiphosphetane (4.0 mMol). The reaction mixture was stirred at room temperature for 2 hours before the precipitate was filtered and washed several times with CH2Cl2. The GYY4137 product was a white solid (67% yield) and was pure as determined by 1H nuclear magnetic resonance. Working solutions of GYY4137 and NaHS were made immediately prior to experimentation and were sterile-filtered through a 20 µm membrane (Lonza).

2.4 Image analysis

Since epi-detected signal arises from scatterers smaller than the incident wavelength [17], GNS signal was determined using epi-detected FWM images. To ensure the detected signal was from GNS alone and to avoid exciting detecting cellular contributions, the pump and Stokes beams were tuned to 2650 cm^{-1}, away from the CH_2 resonance in the so-called biological "silent region" [21]. In cells, there are no naturally occurring Raman-active molecular vibrations in the silent region, hence the strong signal detected in the epi-direction under these conditions that was significantly more intense than non-resonant cellular contributions was attributed to plasmon-enhanced FWM from GNS alone.

In order to map the GNS signal onto the cellular components, CH_2 contrast was recorded in the forwards direction to provide cell morphology information. The GNS and cell morphology data were then combined using the image analysis software package ImageJ (U.S. National Institutes of Health, U.S.A.) to illustrate the spatial distribution of GNS within the cells, relative to the membrane and other lipid-rich cellular organelles, such as lipid droplets and vesicles.

To compare the relative cell cytoplasm volumes containing signal attributed to GNS, an analysis method was developed. The outlines of each cell membrane in each z-stack slice were determined using the CARS images and recorded in ImageJ using the polygon tool. These outlines were mapped onto the GNS signal image stacks in order to isolate GNS within the cells, and disregard the signal from extracellular GNS. The epi-CARS images taken at 2650 cm^{-1} of GNS-free control cells were used to determine the non-resonant pixel threshold. The number of pixels within each cell with intensities above this threshold was compared with the cell's total number of pixels to give the relative percentage of pixels associated with GNS as a function of cell volume. The energy per cell was calculated using the total pixel dwell time over all scans and the number of pixels within each cell, determined using the cell membrane outlines.

#150556 - $15.00 USD Received 5 Jul 2011; revised 18 Aug 2011; accepted 19 Aug 2011; published 22 Aug 2011

3. Results

3.1 Verification of FWM signal from GNS

SEM images (Hitachi S-3200N) confirmed the diameter and shell integrity of the GNS. Figure 2(A) shows a typical SEM image of GNS spin-coated onto ITO-coated glass substrate. The outer gold shells were uniform and complete with no obvious defects, and the incidence of dimers or trimers was below 2% of the population. Figure 2(B) shows an emission spectrum of GNS illumination from pump and Stokes beams, obtained from a droplet of diluted gold nanoshells spun-coated onto a glass coverslip. The pump and Stokes wavelengths used to obtain spectra from the nanoshells were 924 nm and 1254 nm respectively. These values were chosen for consistency with the excitation wavelengths later used to generate CH_2 contrast of cellular structures. The sample was raster scanned with a combined excitation power at the focus of approximately 3 μW.

The spectrum consists of a broad luminescent background with a strong, narrow signal at 732 nm, corresponding to expected position of the FWM signal at $2\omega_p - \omega_s$. This result is consistent with previous investigations into emission from gold nanostructures in which a broad two-photon luminescent signal was observed with FWM signal at the anti-Stokes wavelength [22,23]. The GNS surface plasmon mode is sufficiently broad to be excited by the pump beam, resulting in enhanced local electro-magnetic fields. A wide range of linear and non-linear effects may be enhanced by coupling with surface plasmon modes. The enhanced fields can allow two-photon absorption, a process that is several orders of magnitude weaker in metals in the absence of a surface plasmon mode, exciting d-band electrons into the sp-band thus generating electron-hole pairs. When electron-hole recombination subsequently occurs, incoherent luminescence is produced.

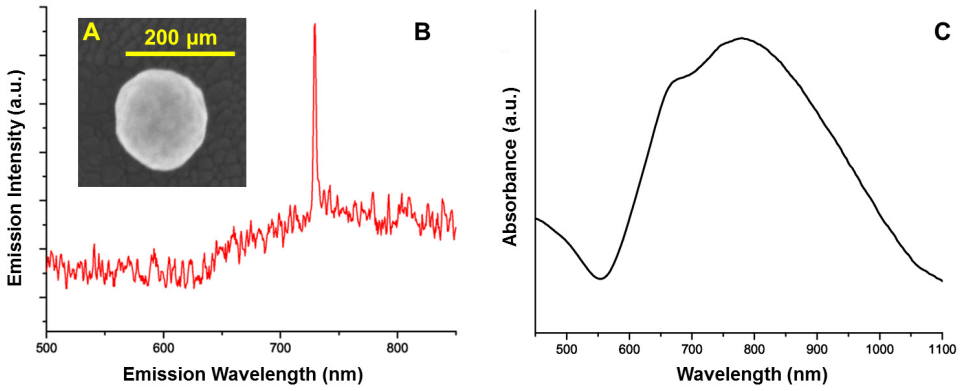

Fig. 2. (A) SEM image of a single gold nanoshell. (B) Luminescence emission spectra of gold nanoshells under excitation from Stokes at 1254 nm and pump at 924 nm simultaneously. (C) UV/vis spectrum of GNS suspended in culture medium.

On the other hand, the coherent FWM signal arises from a plasmon-induced enhancement of gold's third order nonlinear susceptibility [22]. This leads to an intense signal that can be readily isolated from any resonant CARS signals in the surrounding medium by tuning the pump and Stokes away from the resonant wavelengths, a property which makes GNS very attractive as contrast agents in biological samples.

The average of three absorption spectra from GNS suspended in cell culture medium is shown in Fig. 2(C). This spectrum clearly illustrates the broad absorption peak centered at ~785 nm. For both the two pump wavelengths used in FWM imaging (932 nm and 924 nm), the GNS absorbance was 54% and 51% of its peak level respectively.

#150556 - $15.00 USD Received 5 Jul 2011; revised 18 Aug 2011; accepted 19 Aug 2011; published 22 Aug 2011

3.2 Imaging GNS within live cells

Figure 3 demonstrates the technique used to combine the thresholded plasmon-enhanced FWM signal (panels a and d) with the CH_2 CARS signal (panels b and e) to produce a composite image (c and f) showing the location of GNS relative to the cells. The GNS signal was readily separated from non-resonant cell contributions in the epi-direction but not in the forwards direction. This result is as expected, since previous studies of CARS detection in the forwards direction found signal from smaller scatterers tends to be swamped by the signal from larger scatterers, whereas the reverse is true for the epi-direction, with scatterers smaller than the incident wavelengths providing the majority of the detected signal [17].

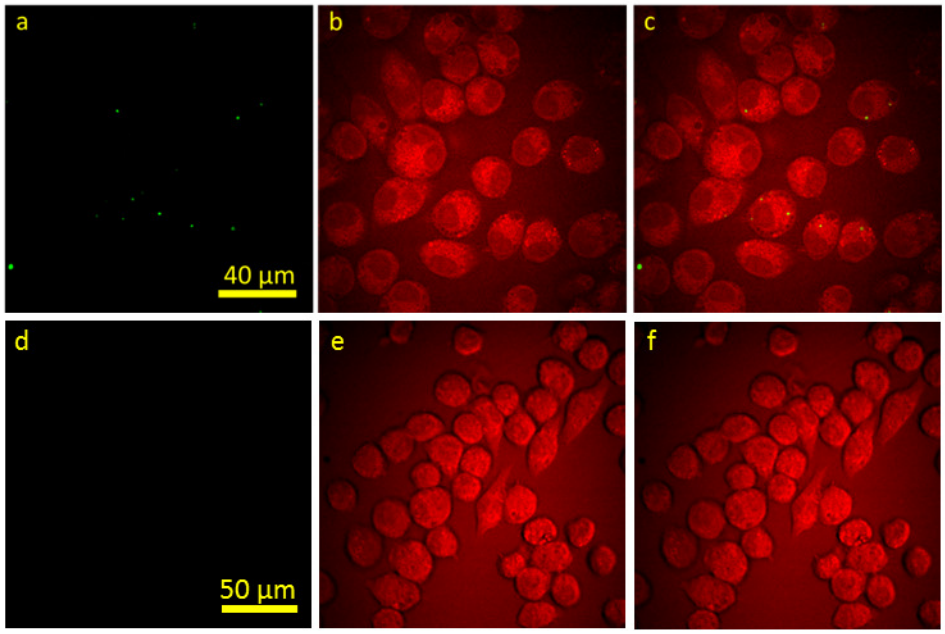

Fig. 3. Epi-detected FWM signal from GNS thresholded to show only pixels above the non-resonant cellular contribution, using pump and Stokes beams tuned to 2650 cm^{-1} (a) and forwards-detected CARS with CH_2 contrast (b) in live cultures of RAW 264.7 cells. Panel (c) is a red/green color composite image using (a) as the green channel and (b) as the red channel. Panels (d) – (f) were obtained in the same manner, using control RAW 264.7 cells that were not exposed to GNS.

Figure 4 shows multi-planar visualizations of typical 3D CARS images stacks of RAW264.7 and A431 cells. Each 2D image consists of 512 x 512 pixels, with a 20 µs dwell time. Each stack consists of 30 images separated by 1 µm. The excitation wavelengths were 924 and 1254 nm for the pump and Stokes beams respectively. The epi- and forwards- FWM images are overlaid (green and red).

Clusters of GNS are visible throughout the cytoplasm of both RAW264.7 and A431 cells, however, none can be found within the nuclei. However, for the RAW264.7 cells GNS were in some cases to be associated with the perinuclear region. Vesicle-encapsulated clusters of GNS were found to range between 0.5 µm (the width of a single pixel) to 5 µm in diameter. Although the corresponding number of GNS comprised within these clusters could not be precisely determined (due to the resolution limit of the microscope and uncertainty associated with determining the signal per nanoshell in a cluster) these volumes give rise to a spatial limit on GNS packing within the clusters of between 19 and several thousand individual GNS.

#150556 - $15.00 USD Received 5 Jul 2011; revised 18 Aug 2011; accepted 19 Aug 2011; published 22 Aug 2011

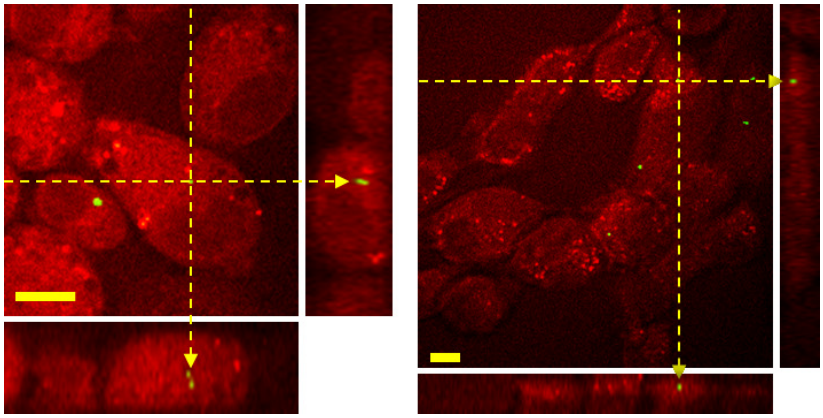

Fig. 4. Spatial distribution of GNS in live cultures of RAW 264.7 (left, Media 1) and A431 (right). Red contrast corresponds with forwards-detected CARS signal with pump and Stokes wavelengths tuned to excite the CH_2 resonance (red). Green signal corresponds with GNS signal. Both bars are 10 μm.

In order to determine the exposure conditions for which FWM imaging of GNS within cells would not induce phototoxic or photothermal effects, the laser power tolerance of cells exposed to the gold nanoshells was compared to that of undosed cells. A minimum of 50 cells were used for each laser power investigated. The total scan time per cell was calculated using the pixel dwell time multiplied by the number of pixels per cell, which in turn was used to determine the laser energy per cell. Control cell cultures that had not been exposed to GNS were imaged in an identical fashion.

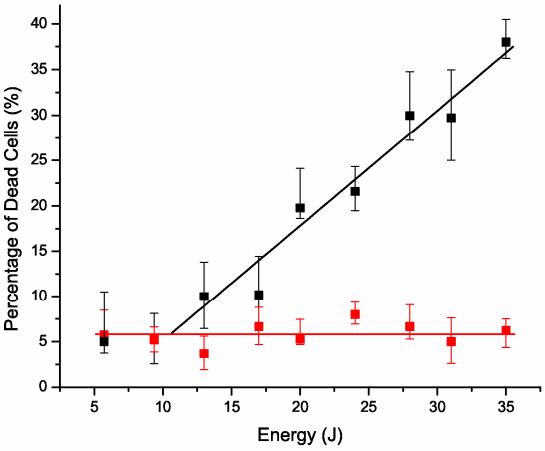

Fig. 5. Graph depicting the percentage of non-viable macrophage cells as a function of laser energy per cell (black line). The baseline mortality exhibited by GNS-free cells exposed to CARS up to 8 mJ per cell at the sample is also shown (red line).

Figure 5 compares cell survival rates for dosed vs. undosed cells as a function of incident laser power. The linear relation between incident laser energy and the percentage of dead cells suggests that the photo-thermal mechanism of induced cell death occurs as a result of a near-SPR single-photon absorption process in the GNS from the pump beam. Under these experimental conditions, we found that cells devoid of GNS were able to withstand exposure to up to 8 mJ per cell without significantly altering their survival rates, whereas cells exposed to GNS displayed a significant increase in cell necrosis over 2.5 mJ per cell.

#150556 - $15.00 USD Received 5 Jul 2011; revised 18 Aug 2011; accepted 19 Aug 2011; published 22 Aug 2011

3.3 The effect of H_2S donor molecule on nanoparticle uptake in macrophage cells

Of the candidate tissues for photothermal therapy with GNS, cancerous tumors are arguably the most medically relevant. Tumors have long been associated with inflammation and an increased number of white blood cells. Since H_2S is known to play an important role in inflammation, we devised a study to demonstrate the applicability of our FWM imaging technique to determine the effect of two H_2S-releasing molecules, NaHS and GYY4137, on the uptake of GNS in live macrophage cultures. We found that the addition of GYY4137 and NaHS to macrophages increased the percentage of the cells containing GNS, as illustrated in Fig. 6, indicating that an increase in H_2S levels in the cell culture medium led to an increase in phagocytosis rates within the macrophages. However, this effect was noticeably more marked with NaHS, which suggests that phagocytosis is dependent on both the concentration and rate of release of H_2S.

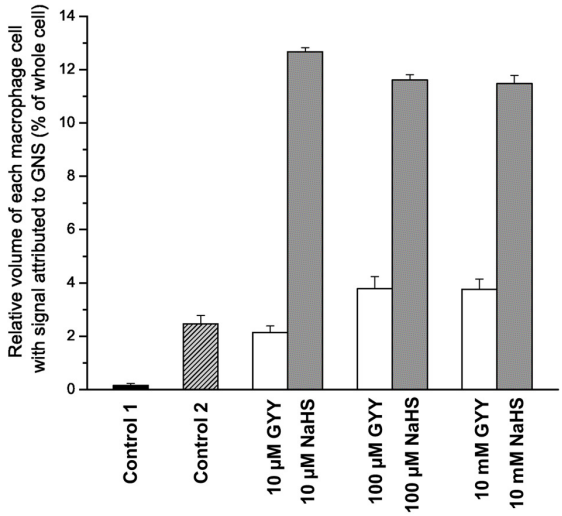

Fig. 6. Effect of H_2S donors on macrophage uptake of GNS. Control 1 corresponds with RAW 264.7 cells unexposed to GNS; control 2 corresponds with RAW 264.7 cells exposed to LPS and GNS but not to any H_2S donor molecules. Between 50 and 100 cells were used for each data point, error bars arise from the standard deviation.

At a molar concentration of 10 µM, GYY4137 added to the cell culture medium resulted in an average GNS pixel percentage of 2.15% +/– 0.25%, which was not statistically significantly lower than the control group which was unexposed to GYY4137 whose GNS pixel percentage as a function of cell volume (PPCV) was 2.47% +/– 0.31%. However for GYY4137 concentrations at 100 µM, the GNS PPCV was 3.78% +/–0.46% (which was significantly greater than the control group, $p< 0.01$), at 1 mM the PPCV was 3.77% +/– 0.38% (which was significantly greater than the control group, $p< 0.01$). This indicates that for GYY4137 levels below 100 µM there is no change in the macrophage's uptake of GNS, whereas for concentrations over this level up to 1 mM there is an associated significant increase in GNS uptake. For all concentrations of NaHS, the increase in GNS PPCV over both the control groups and the GYY4137 groups was statistically significant ($p<0.02$). For NaHS at 10 µM the GNS PPCV was 12.67% +/– 0.15%, dropping to 11.47%. +/– 0.31% for 1 mM.

4. Discussion

Previous studies of gold nano-structures using FWM microscopy have found that the emission spectra obtained from these structures arises from two-photon enhanced luminescence combined with second harmonic generation and coherent anti-Stokes peaks [23]. Our results

#150556 - $15.00 USD Received 5 Jul 2011; revised 18 Aug 2011; accepted 19 Aug 2011; published 22 Aug 2011

indicated that the signal arose from a broad luminescent background with the addition of a strong coherent FWM peak when the GNS were exposed to both Stokes and pump beams. The epi-detected FWM signal from GNS was several orders of magnitude greater than signal arising from epi-detected CARS signal from scatterers smaller than the incident wavelength (such as lipid droplets), as a result of the plasmon-enhancement. This enabled the FWM GNS signal to be readily separated from nonresonant CARS by thresholding the images such that the minimum intensity matched that of the brightest nonresonant cell signal. Using this thresholding technique, multiphoton-induced luminescence from the GNS was not sufficiently intense to allow localization of the particles, whereas FWM signal from the GNS was.

Although the nanoshells' LSPR was tuned to an absorption peak of 785 nm, we found that the peak width was broad enough to enable excitation of plasmon-enhanced FWM using a range of pump and Stokes wavelengths probing Raman shifts at the CH_2 resonance and within the "silent region". We exploited this feature to verify GNS signal within cell cultures by taking sequential FWM images exciting first at the CH_2 resonance to provide contrast from lipid-rich structures, followed by exciting Raman shifts in the "silent region". The epi-detected GNS FWM signal was significantly more intense than the non-resonant CARS contribution from cellular structures. By combining the FWM and CARS data, we were able to determine the spatial localization of GNS within the cells in relation to the lipid membrane and cell nuclei. Although the FWM signal from the GNS would have been greater had we used pump and Stokes beams closer to the plasmon resonance wavelength, the level of intensity achieved in our experiments was more than sufficient. Additionally, imaging with the pump beam at the plasmon resonance would reduce the damage threshold to the point where sufficient CARS contrast could not be obtained and could cause damage to the GNS. Hence, the limiting factor to the quality of our images was the intensity of CARS signal and not the FWM GNS signal.

We chose a pixel dwell time of ~20 µs, giving scan rates of ~5 seconds per frame, as this was slow enough to provide sufficiently high levels of CARS and FWM contrast without causing damage to the cells, whilst being fast enough to reduce the potential of motion artifacts brought about by the cells moving between images. When imaging at these scan rates, we found signal from GNS within the cell cytoplasm enclosed in vesicles in clusters ranging from approximately 0.5 µm to 5 µm in diameter. When nanoshells cluster, they exhibit changes in their plasmon resonance wavelength that are dependent on the number of nanoshells and their spacing within the cluster. Previous studies of this effect in 3-D clusters have found a blue-shift of the resonance when the ratio of inter-particle spacing to particle diameter increases [24]. In our experiment this would manifest itself as a change in GNS FWM intensity. However, the shifts in plasmon resonance of clusters were not found to be sufficient to reduce the FWM signal to the point where it could no longer be separated from the nonresonant CARS signal. We found that macrophage cells tended to contain between 1 and 5 clusters when exposed to GNS at a concentration of 6×10^7 per mL in their cell culture medium for 24 hours prior to imaging. Cancer cells were found to contain fewer clusters, with a higher incidence of GNS-free cells than for macrophages. For both cell types, GNS were found throughout the cytoplasm and in the perinuclear region, but not within the nucleus itself.

We demonstrated the applicability of the signal isolation technique to particle uptake investigations in a study of the effects of hydrogen sulfide. Hydrogen sulfide is a chemical produced in a variety of mammalian tissues, such as the liver, lung, pancreas, brain, colon etc. Much work is being undertaken to determine the biological roles of H_2S, particularly regarding its role in inflammation. There are much conflicting data on this topic, further complicated by the ability of H_2S to affect the bioavailability of another chemical involved in inflammation, NO. Traditional hydrogen sulfide donors, such as NaHS, release H_2S rapidly in aqueous solution. Such high concentrations of H_2S released over short time periods are unsuitable for determining the biological effects of H_2S on live cells as they are not

#150556 - $15.00 USD Received 5 Jul 2011; revised 18 Aug 2011; accepted 19 Aug 2011; published 22 Aug 2011

comparable with conditions found within tissues where levels of H_2S are only ever found to change slowly.

We used FWM microscopy to investigate the effect of a slow-release H_2S donor (GYY4137) and a fast-release H_2S donor (NaHS) on the uptake of GNS into macrophage cells. GYY4137 is preferable to more "conventional" H_2S donors such as NaHS, as it has been found to release H_2S slowly in aqueous solution in vitro, producing biological effects that are more comparable to those arising from endogenous H_2S. We found that nanoparticle uptake in white blood cells drastically increased relative to the control group when the cultures were exposed to NaHS, indicating that an increase in free H_2S leads to an increased phagocytic response. An increase in nanoparticle uptake was also observed for the slow-release H_2S donor GYY4137 although this was much less marked than for the rapid-release donor. These results suggest that both the rate of release and the concentration of H_2S in the cell culture medium affect the rate of phagocytosis.

Determining dose and uptake mechanisms at the cellular level is a crucial step towards bringing new nanoparticle-based therapies out of the laboratory and into the hospital. Our study has shown that using FWM microscopy it is possible to selectively determine relative gold nanoshell uptake in live cells and induce localized GNS-mediated photo-thermal effects leading to cell death. We found that the percentage of cells exhibiting membrane damage as a result of GNS-heating increased linearly with incident laser energy on the sample over a threshold. Moreover, we have demonstrated the applicability of this imaging system to investigations of factors affecting particle uptake in live cells.

5. Conclusions

Our experiments have shown that GNS make excellent contrast agents for FWM microscopy of live cell cultures. The signal obtained from GNS under FWM excitation conditions was found to arise from a broad multi-photon enhanced luminescence with a strong FWM peak at the anti-Stokes wavelength. Since GNS heat rapidly upon excitation at their plasmon resonance wavelength, a power study was performed to determine the optimum laser power for imaging cells containing GNS without causing membrane damage or cell death. We determined that when the total laser energy incident on each cell exceeded 2.5 mJ, the cells exhibited higher than background levels of cell death, as determined using a Trypan blue vital stain study. Above this threshold, the cell death levels were found to increase linearly with incident laser power.

When imaging cell cultures exposed to GNS, the intensity of the GNS signal was found to be several orders of magnitude greater than that of the resonant CARS signal from lipid droplets within the cells. This enhanced GNS signal was therefore readily separable from the non-GNS signal using simple image thresholding techniques, thus allowing precise spatial localization of the GNS within each cell. This spatial localization method was used to determine the relative change in uptake of GNS for live macrophage cells exposed to one of two H_2S donor molecules, NaHS and GYY4137. We found that the rapidly-releasing H_2S donor molecule, NaHS resulted in GNS uptake levels that far exceeded those for the slowly-releasing donor molecule, GYY4137. These findings have important implications for studies investigating the effect of H_2S on phagocytosis of nanoparticles.

Acknowledgments

This work was funded by the UK Engineering and Physical Sciences Research Council (EPSRC). Many thanks to Dr. Andreas Schatzlein, and Dr. Maria Fuente from the London School of Pharmacy for help and advice on cell culture.

#150556 - $15.00 USD Received 5 Jul 2011; revised 18 Aug 2011; accepted 19 Aug 2011; published 22 Aug 2011